

DEVELOPMENT OF SUPERCAPACITORS
WITH IN-SITU POLYMERIZED POLYANILINE
ON MnO_2 AND Co_3O_4 ANODES AND
ACTIVATED CARBON CATHODES

IZAN IZWAN BIN MISNON

DOCTOR OF PHILOSOPHY
UNIVERSITI MALAYSIA PAHANG

**THESIS CONFIDENTIAL STATUS
UNIVERSITI MALAYSIA PAHANG**

DECLARATION OF THESIS AND COPYRIGHT

Author's full name : Izan Izwan Bin Misnon

Date of birth : 3 December 1983

Title : Development of Supercapacitors with In-Situ Polymerized
Polyaniline on MnO₂ and Co₃O₄ Anodes and Activated
Carbon Cathodes

Academic Session : Semester II 2015/2016

I declare that this thesis is classified as:

CONFIDENTIAL (Contains confidential information under the
Official Secret Act 1972)

RESTRICTED (Contains restricted information as specified by
the organization where research was done)

OPEN ACCESS I agree that my thesis to be published as online
open access (Full text)

I acknowledge that Universiti Malaysia Pahang reserve the right as follows:

1. The Thesis is the Property of Universiti Malaysia Pahang
2. The Library of Universiti Malaysia Pahang has the right to make copies for the purpose of research only.
3. The Library has the right to make copies of the thesis for academic exchange.

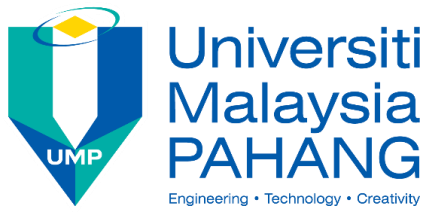
Certified By:

(Student's Signature)

Izan Izwan Bin Misnon
831203-10-5783
Date:

(Supervisor's Signature)

Prof. Dr. Jose Rajan
Date:



SUPERVISORS' DECLARATION

I hereby declare that I have checked the thesis and in my opinion, this thesis is adequate in terms of scope and quality for the award of the degree of Doctor of Philosophy (Advanced Materials).

Signature

Name of Supervisor : PROF. DR. JOSE RAJAN

Position : PROFESSOR

Date :



STUDENT'S DECLARATION

I hereby declare that the work in this thesis is my own except for quotations and summaries which have been duly acknowledged. The thesis has not been accepted for any degree and is not concurrently submitted for award of other degree.

Signature :
Name : IZAN IZWAN BIN MISNON
ID Number : PSM11002
Date :

DEVELOPMENT OF SUPERCAPACITORS WITH IN-SITU POLYMERIZED
POLYANILINE ON MnO_2 AND Co_3O_4 ANODES AND ACTIVATED CARBON
CATHODES

IZAN IZWAN BIN MISNON

Thesis submitted in fulfillment of the requirements for the
award of the degree of Doctor of Philosophy

Faculty of Industrial Sciences & Technology
UNIVERSITI MALAYSIA PAHANG

AUGUST 2016

TABLE OF CONTENTS

	Page
DEDICATION	i
ACKNOWLEDGEMENTS	ii
ABSTRACT	iii
ABSTRAK	iv
TABLE OF CONTENTS	v
LIST OF TABLES	x
LIST OF FIGURES	xiii
LIST OF SYMBOLS/UNITS	xxiii
LIST OF ABBREVIATIONS	xxv
CHAPTER 1 INTRODUCTION	1
1.1 ENERGY DEMAND AND ENERGY STORAGE SCENARIO	1
1.2 PROBLEM STATEMENT	3
1.3 OBJECTIVES OF RESEARCH	4
1.4 SCOPE OF RESEARCH	4
1.5 STATEMENT OF CONTRIBUTION	6
1.6 OUTLINE OF THE THESIS	7
CHAPTER 2 LITERATURE REVIEW	8
2.1 INTRODUCTION	8
2.2 HISTORY OF SUPERCAPACITORS DEVELOPMENT	8
2.3 SUPERCAPACITOR AS ENERGY STORAGE DEVICE	10
2.4 CLASSIFICATION (TAXONOMY) OF SUPERCAPACITORS BASED ON FUNDAMENTAL OPERATING PROCESS	13
2.4.1 Electrochemical Double Layer Capacitors Charge Storage Mechanism	14
2.4.2 Pseudocapacitance Charge Storage Mechanism	17
2.4.3 Comparison of EDLC and PC mechanisms	19

2.5	IMPROVING ENERGY DENSITY BY ASYMMETRIC DEVICE STRUCTURE	20
2.6	MATERIALS FOR SUPERCAPACITORS	21
2.6.1	PC Materials	23
2.6.2	EDLC Materials	37
2.7	CONCLUSIONS	40
CHAPTER 3 MATERIALS AND METHODS		42
3.1	INTRODUCTION	42
3.2	RESEARCH METHODOLOGY	42
3.3	MATERIAL SYNTHESIS METHODS	44
3.3.1	Hydrothermal Synthesis	44
3.3.2	Molten Salt Synthesis	44
3.3.3	Polyaniline Nanocomposites Synthesis	45
3.3.4	Synthesis of Activated Carbon from Palm Kernel Shells	46
3.4	MATERIAL CHARACTERIZATIONS	46
3.4.1	X-ray Diffractometer	46
3.4.2	Thermogravimetric Analysis	49
3.4.3	Fourier Transformed Infrared spectroscopy	51
3.4.4	Gas adsorption analyses	52
3.4.5	Field Emission Scanning Electron Microscope	55
3.4.6	Transmission Electron Microscope	56
3.5	ELECTRODE FABRICATION	58
3.6	ELECTROCHEMICAL ANALYSES	58
3.6.1	Test Cell Configuration	59
3.6.2	Cyclic Voltammetry	60
3.6.3	Galvanostatic Charge Discharge	62
3.6.4	Electrochemical Impedance Spectroscopy	62
3.6.5	Cycle Stability Test	65

CHAPTER 4 SYNTHESIS AND CHARACTERIZATION OF MANGANESE OXIDE AND COBALT OXIDE AND THEIR POLYMERIC COMPOSITES	66
4.1 INTRODUCTION	66
4.2 SYNTHESIS OF MANGANESE OXIDE AND COBALT OXIDE USING HYDROTHERMAL METHOD	66
4.3 SYNTHESIS OF MANGANESE OXIDE AND COBALT OXIDE USING MSS METHOD	67
4.4 SYNTHESIS OF POLYANILINE COMPOSITES	67
4.5 PHYSICOCHEMICAL CHARACTERIZATIONS	68
4.5.1 X-Ray Diffraction Analysis	68
4.5.2 Thermogravimetric Analysis	73
4.5.3 FTIR Analysis	76
4.5.4 FESEM Analysis	79
4.5.5 TEM Analysis	81
4.5.6 BET Analysis	84
4.6 CONCLUSION	88
CHAPTER 5 RATIONALE OF ELECTROLYTE SELECTION FOR MAXIMIZING ARCHIEVABLE CAPACITANCE IN A SUPERCAPACITOR ELECTRODES	89
5.1 INTRODUCTION	89
5.2 ELECTROCHEMICAL ANALYSIS OF MANGANESE OXIDE IN THREE-ELECTRODE CONFIGURATION	90
5.2.1 Cyclic Voltammetry Analysis	90
5.2.2 Galvanostatic Charge Discharge Analysis	92
5.2.3 Electrochemical Impedance Spectroscopy Analysis	93
5.3 CONCLUSION	97

CHAPTER 6 ELECTROCHEMICAL EVALUATION OF MANGANESE OXIDE AND COBALT OXIDE AND THEIR POLYANILINE COMPOSITES	98
6.1 INTRODUCTION	98
6.2 ELECTROCHEMICAL EVALUATION OF MANGANESE OXIDE, COBALT OXIDE AND THE EFFECT OF PANI MODIFICATION	98
6.2.1 Cyclic Voltammetry Analyses	98
6.2.2 Galvanostatic Charge Discharge Analyses	110
6.2.3 Electrochemical Impedance Spectroscopy Analysis	116
6.3 CONCLUSIONS	120
CHAPTER 7 ELECTROCHEMICAL PERFORMANCE OF ACTIVATED CARBON FROM PALM KERNEL SHELL BIOWASTE	121
7.1 INTRODUCTION	121
7.2 EXPERIMENTAL	121
7.2.1 Material Synthesis	121
7.3 RESULT AND DISCUSSION	122
7.3.1 XRD Analysis	122
7.3.2 FTIR Analysis	124
7.3.3 Gas Adsorption Analysis	125
7.3.4 FESEM Analysis	126
7.4 CAPACITIVE PERFORMANCE OF CHEMICAL AND PHYSICAL ACTIVATION OF PKS	127
7.4.1 CV and Galvanostatic CDC cycling	127
7.4.2 Electrochemical Impedance Spectroscopy Analysis	132
7.5 CONCLUSION	135
CHAPTER 8 CHARACTERISTICS OF SYMMETRIC AND ASYMMETRIC SUPERCAPACITOR BASED ON CARBON AND POLYMER COMPOSITES	136
8.1 INTRODUCTION	136

8.2	SYMMETRIC SUPERCAPACITORS USING PKS DERIVED ACTIVATED CARBON	136
8.2.1	Optimization of Cell Potential for SSC Fabrication	137
8.2.2	Cyclic Voltammetry Analysis for SSC device	139
8.2.3	Effect of Electrolyte on the SSC Derived PKS AC	140
8.2.4	SSC Performance and Cell Stability Test	142
8.2.5	Comparison of SSC and ASC Performance With Commercial Carbon	145
8.3	ASYMMETRIC SUPERCAPACITORS USING PSEUDOCAPACITIVE COMPOSITE MATERIALS	148
8.3.1	Electrode Optimization	148
8.3.2	Cyclic Voltammetry Analysis of ASCs	150
8.3.3	Galvanostatic Charge Discharge Studies for ASC Cell	152
8.3.4	Electrochemical Impedance Spectroscopy Analysis	155
8.3.5	Stability Test of ASC Cell	156
8.3.6	Ragone Plot and Comparison of ASC Cell	157
8.4	CONCLUSION	159
CHAPTER 9 SUMMARY AND RECOMMENDATIONS		161
9.1	SUMMARY	161
9.2	RECOMMENDATIONS FOR FUTURE RESEARCH	164
REFERENCE		166
APPENDIX A XPS ANALYSIS OF PKS AC		186
APPENDIX B ARCHIEVEMENTS		187

LIST OF TABLES

Table No.	Title	Page
2.1	Device properties comparison of capacitors, SCs and batteries	11
2.2	The EDLC and PC mechanism comparison	19
2.3	General characteristics of common SCs electrode materials	22
2.4	Brief summary of research on the use of RuO ₂ nanostructures and their composites as a SCs electrode	26
2.5	The build up structure of MnO ₂	29
2.6	A brief summary of MnO ₂ nanostructures and their composites as a SCs electrode	29
2.7	A brief summary of Co ₃ O ₄ nanostructures and their composites as a SCs electrode	33
2.8	A brief summary of CPs and TMOs composite as a SCs electrode	36
2.9	Comparison of activated carbon derived from biomass precursor	39
4.1	XRD data of MnH	70
4.2	XRD data of MnM	71
4.3	XRD data of CoH	71
4.4	XRD data of CoM	72
4.5	Average crystallite size and d-spacing of prepared sample	72
4.6	The amount of PANI loaded onto the metal oxide composites	75

4.7	The vibrational modes for all sample	77
4.8	The tabulated surface properties of the studies materials determined from BET analysis	88
5.1	The value of R_S , R_{ct} , R_d and τ for all electrolytes	94
6.1	Variation of C_S for MnO_2 and Co_3O_4 and their PANI composites electrodes	103
6.2	Diffusion coefficients of the electrodes	105
6.3	Extracted data for surface PCs and total PCs on each electrode	108
6.4	The q_T^* , q_o^* and q_i^* evaluation for all electrodes	110
6.5	Variation of C_S for MnO_2 and Co_3O_4 and their PANI composites electrodes analyzed from CDC	113
6.6	Effect of PANI on the electrode resistance at current density 1 A g^{-1}	114
6.7	Performance comparison of some conducting polymer nanocomposite in aqueous electrolyte	115
6.8	The R_S , R_{ct} , R_d and τ value extracted from EIS analysis	117
7.1	Results of Debye – Scherrer analysis of the AC	123
7.2	Nitrogen adsorption–desorption data for the two AC	125
7.3	Electrochemical performance of AC-C and AC-P electrodes	131
8.1	Specific capacitance at different current density for AC-C and AC-P cell in 1M H_2SO_4 , 1M Na_2SO_4 and 6M KOH electrolytes	141

8.2	Ion radius, solvated ion radius, molar conductivity and ionic mobility of electrolyte ions	142
8.3	Nitrogen adsorption–desorption data for AC-C, AC and OMC	147
8.4	Calculation of mass ratio for ASCs fabrication	150
8.5	C_S of PANI-Mn and PANI-Co at different carbon electrode	151
8.6	The R_S , R_{ct} , and R_d of ASCs determine from EIS analysis	156
8.7	Comparison of ASCs with recent asymmetric configuration design	159

LIST OF FIGURES

Figure No.	Title	Page
2.1	Development eras for SCs technologies	9
2.2	Supercapacitor mechanism during charging and discharging process	11
2.3	Ragone plot of capacitors, SCs and batteries	12
2.4	Number of papers published in the area of Science Technology between 2000 and 2015 generated from ISI web of science using the keywords ‘supercapacitors’ OR ‘electrochemical capacitors’ on 21 May 2015	12
2.5	Classification of SCs based on operating mechanism	14
2.6	Schematic diagrams of (a) Helmholtz Model; (b) Gouy-Chapman Model, (c) Stern Model and (d) Grahame Model	15
2.7	(a) Adsorption, (b) redox and (c) doping–dedoping mechanism for PC material	17
2.8	Strategies adapted by researchers to produce high ED in SCs fabrication	20
2.9	Performance comparison on different types of SCs materials	23
2.10	The rutile crystal structure showing bond distances of anhydrous RuO ₂	24
2.11	The (a) polycrystalline, (b) nanorod, (c) nanotube, (d) nanowire, (e) cauliflower and (f) nanoplate morphologies of RuO ₂	25
2.12	Allotrope of MnO ₂ in α –, β –, γ –, δ – and λ – form	27

2.13	The (a) flower/plate, (b) nanorod, (c) hollow sphere/urchin, (d) cubic, (e) nanowires and (f) lamellar morphologies of MnO ₂	28
2.14	Crystal structure of Co ₃ O ₄	31
2.15	The (a) nanosheet, (b) layered, (c) nanocubes, (d) dumbbell, (e) nanotubes and (f) hollow-sphere morphologies of Co ₃ O ₄	32
2.16	Chemical structure of (a) PTh, (b) PPy, (c) PEDOT and (d) PANI.	34
2.17	Electron hooping on CPs conjugated double bonds	35
2.18	Redox state of PANI	35
3.1	Summary of methodology adopted by this work	43
3.2	(a) A basic hydrothermal reactor set-up with capacity of 250 mL and (b) schematic diagram of nucleation growth inside reactor	45
3.3	The (a) photograph and (b) basic schematic diagram of XRD machine	47
3.4	The conventional derivation of Bragg's Law in X-ray diffraction	48
3.5	The (a) photograph and (b) schematic diagram of TG instrument	50
3.6	Typical data of TG and DTG curves	50
3.7	FTIR spectrometer diagram	52
3.8	The (a) photograph and (b) schematic diagram of gas adsorption analysis machine	53

3.9	Type of hysteresis loop according to IUPAC classification	54
3.10	(a) FESEM instrument, (b) schematic diagram of FESEM and (c) generation of x-ray and secondary electron from electrons beam	56
3.11	(a) TEM instrument and (b) schematic diagram of TEM	57
3.12	(a) Photograph of potentiostat–galvanostat instrument and (b) schematic diagram of potentiostat–galvanostat circuit	59
3.13	Three electrode configuration set-up for electrochemical analysis	60
3.14	Two electrode configuration set-up for electrochemical analysis	60
3.15	Typical CV curves showing relation of v with i	61
3.16	Typical Nyquist plot in EIS analysis	63
3.17	Battery testing machine	65
4.1	X-ray diffractograms of (a) MnH, (b) MnM, (c) CoH and (d) CoM	69
4.2	X-ray diffractograms of (a) PANI-MnH, (b) PANI-MnM, (c) PANI-CoH and (d) PANI-CoM	70
4.3	TG and DTG curve of (a) MnH, (b) PANI-MnH, (c) MnM, (d) PANI-MnM, (e) CoH, (f) PANI-CoH, (g) CoM and (h) PANI-CoM under nitrogen at a heating rate $10\text{ }^{\circ}\text{C min}^{-1}$	74
4.4	FTIR spectra of (a) MnH, (b) MnM, (c) CoH and (d) CoM	76
4.5	FTIR spectra of (a) PANI-MnH, (b) PANI-MnM, (c) PANI-CoH, (d) PANI-CoM and (e) PANI	78

4.6	FESEM micrographs for (a) MnH, (b) PANI-MnH, (c) MnM, (d) PANI-MnM, (e) CoH, (f) PANI-CoH, (g) CoM and (h) PANI-CoM	80
4.7	TEM (a1 & a2) and HRTEM (b1 & b2) images for MnH and PANI-MnH respectively	81
4.8	TEM (a1 & a2) and HRTEM (b1 & b2) images for MnM and PANI-MnM respectively	82
4.9	TEM (a1 & a2) and HRTEM (b1 & b2) images for CoH and PANI-CoH respectively	83
4.10	TEM (a1 & a2) and HRTEM (b1 & b2) images for CoM and PANI-CoM respectively	84
4.11	Nitrogen adsorption-desorption isotherm for (a) MnH and PANI-MnH, (b) MnM and PANI-MnM, (c) CoH and PANI-CoH and (d) CoM and PANI-CoM respectively	87
5.1	Typical CV curve for MnH electrode in (a) LiOH, (b) NaOH and (c) KOH electrolytes	91
5.2	The CV CS variations of MnH electrode at different electrolytes	92
5.3	(a) Typical CDC curve of MnH electrode at various current densities in LiOH electrolyte; the arrow indicates the increasing discharge time with decrease in current density; (b) Galvanostatic CDC analysis at various current densities	92
5.4	Nyquist plots of the MnH at different electrolytes showing the first semicircle at the high – mid frequency region	94

5.5	(a) The plot of Z' vs. $1/\omega^{1/2}$; (b) The variations of the real part of capacitance (C') of MnH in different electrolytes; (c) The variations of the imaginary part of capacitance (C'') of MnH in different electrolytes	95
5.6	FESEM micrograph of MnH electrode at (a) cross section of electrode-composite and (b) mixed composite of active material	97
6.1	CV curve for (a) MnH and PANI-MnH, (b) MnM and PANI-MnM; two distinct redox peaks for MnO_2 was observed, (c) CoH and PANI-CoH; two distinct redox peaks for Co_3O_4 was observed, and (d) CoM and PANI-CoM at a scan rate of 2 mV s^{-1}	99
6.2	CV curve for (a) MnH and (b) PANI-MnH in scan rate range $2 - 40 \text{ mV s}^{-1}$	101
6.3	CV curve for (a) MnM and (b) PANI-MnM in scan rate range $2 - 40 \text{ mV s}^{-1}$	101
6.4	CV curve for (a) CoH and (b) PANI-CoH in scan rate range $2 - 40 \text{ mV s}^{-1}$	102
6.5	CV curve for (a) CoM and (b) PANI-CoM in scan rate range $2 - 40 \text{ mV s}^{-1}$	102
6.6	Plot of CS versus scan rate for all electrodes in 6 M KOH electrolyte	103
6.7	The i_p versus \sqrt{v} linear plot of (a) MnH and PANI-MnH, (b) MnM and PANI-MnM, (c) CoH and PANI-COH and (d) CoM and PANI-CoM	104

6.8	Plot of (a) peak current density versus v and (b) peak current density versus $v^{-1/2}$ of each electrode based on CV performance to determine the PCs mechanism on the electrode surfaces. On the caption panel, A and C is corresponds to anodic and cathodic scan respectively	106
6.9	Plot of (a) C_S versus $v^{-1/2}$ and (b) C_S^{-1} versus $v^{1/2}$ of each electrode based on CV performance to determine the surface contribution to PCs compared to the total C_S	107
6.10	Charge vs. square root of scan rate for and charge vs. inverse square root of scan rate plot of MnH and PANI-MnH (a,b), MnM and PANI-MnM (c,d), CoH and PANI-CoH (e,f) and CoM and PANI-CoM (g,h)	109
6.11	CDC curve for (a) MnH and PANI-MnH; IR drop observed during discharging, (b) MnM and PANI-MnM, (c) CoH and PANI-CoH, and (d) CoM and PANI-CoM at a current density of 1 A g^{-1}	111
6.12	Discharge curve of (a) MnH and (b) PANI-MnH at $10 - 0.5 \text{ A g}^{-1}$	111
6.13	Discharge curve of (a) MnM and (b) PANI-MnM at $10 - 0.5 \text{ A g}^{-1}$	112
6.14	Discharge curve of (a) CoH and (b) PANI-CoH at $10 - 0.5 \text{ A g}^{-1}$	112
6.15	Discharge curve of (a) CoM and (b) PANI-CoM at $10 - 0.5 \text{ A g}^{-1}$	112
6.16	Plot of C_S versus current density for all electrodes in 6 M KOH electrolyte	113

6.17	(a) EIS, (b) Bode and (c) real and imaginary plots of MnH and PANI-MnH electrodes	116
6.18	(a) EIS, (b) Bode and (c) real and imaginary plots of MnM and PANI-MnM electrodes	118
6.19	(a) EIS, (b) Bode and (c) real and imaginary plots of CoH and PANI-CoH electrodes	119
6.20	(a) EIS, (b) Bode and (c) real and imaginary plots of CoM and PANI-CoM electrodes	119
7.1	XRD patterns of (a) AC-C and (b) AC-P	123
7.2	FTIR spectra for (a) AC-C and (b) AC-P	124
7.3	Nitrogen adsorption/desorption isotherm for (a) AC-C and (b) AC-P samples. Insets are the pore size distribution for each AC	126
7.4	FESEM micrograph for AC-C (a,b) and AC-P (c,d) at low and high magnifications	127
7.5	CV curve of (a) AC-C and (b) AC-P in 1 M KOH at scan rate from 10 to 150 mV s ⁻¹ ; (c) Comparison of CV curves for AC-C and AC-P at scan rate 10 mV s ⁻¹ and (d) dependence of C _S on the scan rate of CV	128
7.6	Dependency pattern of volumetric current versus scan rate for (a) AC-C and (b) AC-P samples	129
7.7	The CDC behavior of (a) AC-C and (b) AC-P electrode in 1 M KOH electrolyte at potential window -1.0 to 0.0 V; (c) CDC curve for AC at 1 A g ⁻¹ ; (d) C _S at various current densities	130
7.8	Stability test of AC electrodes at current density 5 A g ⁻¹	132

7.9	(a) Nyquist plot of AC electrodes, Inset: a magnified portion at high frequency showing R_S and R_d ; (b) Bode phase plot of AC electrodes; (c) Imaginary capacitance versus frequency of AC electrodes	133
8.1	(a) CDC curve of AC-C, (b) CDC curve of AC-P and (c) C_S and Coulombic efficiency relation of AC-C and AC-P device in 1M H_2SO_4 electrolyte. The analysis conducted at 1 A g^{-1} at potential range 0.6 – 1.2 V	138
8.2	(a) CDC curve of AC-C, (b) CDC curve of AC-P and (c) C_S and Coulombic efficiency relation of AC-C and AC-P device in 1M Na_2SO_4 electrolyte. The analysis conducted at 1 A g^{-1} at potential range 1.2 – 2.2 V	138
8.3	(a) CDC curve of AC-C, (b) CDC curve of AC-P and (c) C_S and Coulombic efficiency relation of AC-C and AC-P device in 6M KOH electrolyte. The analysis conducted at 1 A g^{-1} at potential range 0.8 – 1.4 V	139
8.4	CV curve of SSC cell in the scan rate range of 10 – 100 mV s^{-1} . The CV curve for (a1) AC-C and (a2) AC-P cell in 1M H_2SO_4 electrolyte; CV curve for (b1) AC-C and (b2) AC-P cell in 1M Na_2SO_4 electrolyte; CV curve for (c1) AC-C and (c2) AC-P cell in 6M KOH electrolyte	140
8.5	Ragone plot of different types of electrolyte	143
8.6	(a) curve for AC-C cell in H_2SO_4 electrolyte at CDC cycle 3100 – 3120, CDC cycle of SSC at optimized working potential at current density 0.5 A g^{-1} for (b) H_2SO_4 , (c) Na_2SO_4 , (d) KOH electrolytes	144
8.7	Typical CDC curve of SSC cell for AC//AC and OMC//OMC	146

8.8	(a) Variation of CS of different SSC cell at current density range 0.5–5 A g ⁻¹ and (b) Ragone plot for SSC cell for cathode comparison	146
8.9	Nitrogen adsorption–desorption isotherm for commercial (a) AC and (b) OMC. Inset are the pore size distribution of each carbon	147
8.10	CV curves for anodes (PANI composite – right) and cathodes (carbon – left) individual scan at 10 mV s ⁻¹	149
8.11	CV curve for (a) PANI-Co and (b) PANI-Mn in different carbon electrode at scan rate of 10 mV s ⁻¹	151
8.12	(a) CDC curve for PANI-CoH//AC and PANI-CoH//OMC and (b) CDC curve for PANI-MnM//AC and PANI-MnM//OMC at current density 1 A g ⁻¹	152
8.13	Discharge curve of ASCs for (a) PANI-MnH//AC, (b) PANI-MnH//OMC, (c) PANI-MnM//AC and (d) PANI-MnM//OMC. The CDC analysis was conducted at current density range 0.5 – 5 A g ⁻¹	153
8.14	Discharge curve of ASCs for (a) PANI-CoH//AC, (b) PANI-CoH//OMC, (c) PANI-CoM//AC and (d) PANI-CoM//OMC. The CDC analysis was conducted at current density range 0.5 – 5 A g ⁻¹	154
8.15	Variation of C _s in CDC analysis at current density range 0.5 – 5 A g ⁻¹ for (a) PANI-Mn and (b) PANI-Co ASCs	154
8.16	(a) Nyquist plot of PANI-Mn ASCs; inset is magnified high-medium region of Nyquist plot, and (b) Bode plot of the ASCs	155

8.17	(a) Nyquist plot of PANI-Co ASCs; inset is magnified high-medium region of Nyquist plot, and (b) Bode plot of the ASCs	156
8.18	Stability test at current density 0.5 A g ⁻¹ for (a) PANI-Mn series and (b) PANI-Co series for 5000 cycles	157
8.19	Ragone plot for (a) PANI-Mn and (b) PANI-Co ASCs series using different cathode	158

LIST OF SYMBOLS/UNITS

\sim	approximately
%	percent
λ	wavelength
μ	micron (10^{-6})
η	coulombic efficiency
τ	dielectric relaxation time constant
2θ	Bragg angle
$^{\circ}\text{C}$	degree celcius
\AA	angstrom (10^{-10})
A g^{-1}	ampere per gram
a.u.	arbitrary unit
C g^{-1}	charge per gram
C'	real capacitance
C''	imaginary capacitance
$\text{Cu K}\alpha$	X-ray diffraction from copper K energy levels
cm^{-1}	per centimeter
C_s	specific capacitance
d	distance
D	diffusion coefficient
D_{K^+}	potassium ion diffusion
e.g.	<i>exempli gratia</i> (example)
<i>et al.</i>	<i>et alii</i> (and others)
E	potential
E_D	energy density
F g^{-1}	farad per gram
g	grams
h	hour
i.e.	<i>id est</i> (that is)
i_p	peak current
j	current density
L	thickness of electrode film

$\text{m}^2 \text{g}^{-1}$	meter square per gram
M	molar (mol/L)
min	minute
mol	mol
mL	milliliter
mV s^{-1}	millivolt per second
n.a.	not available
NR	not reported
nm	nanometer (10^{-9})
P/P_0	relative pressure; obtained by forming the ratio of the equilibrium pressure and vapour pressure P_0 of the adsorbate at the temperature where the isotherm is measured
P_D	power density
ppm	part per million
q_i	inner charge
q_o	outer charge
q_T	total charge
R_{ct}	charge transfer resistance
R_d	diffusion resistance
R_s	series resistance
S cm^{-1}	Siemen per centimeter
t	time
t_c	charging time
t_d	discharging time
v	scan rate
V	voltage
viz.	<i>videlicet</i> (namely)
wt %	weight percentage
W kg^{-1}	watt per kilogram
Wh kg^{-1}	watt hour per kilogram
Z'	real impedance
Z''	imaginary impedance

LIST OF ABBREVIATIONS

AC	activated carbon
AC-C	chemically modified activated carbon
AC-P	physically modified activated carbon
ASC	asymmetric supercapacitor
CDC	charge discharge
CoH	hydrothermal synthesized cobalt oxide
CoM	molten salt synthesized cobalt oxide
CP	conducting polymer
CV	cyclic voltammetry
EIS	electrochemical impedance spectroscopy
EDLC	electrochemical double layer capacitance
FESEM	field emission scanning electron microscope
FTIR	Fourier transform infrared
IHP	inner Helmholtz plane
MnH	hydrothermal synthesized manganese oxide
MnM	molten salt synthesized manganese oxide
MSS	molten salt synthesis
OHP	outer Helmholtz plane
LIB	lithium ion batteries
PKS	palm kernel shell
PANI	polyaniline
PANI-CoH	polyaniline composite with hydrothermal synthesized cobalt oxide
PANI-CoM	polyaniline composite with molten salt synthesized cobalt oxide
PANI-MnH	polyaniline composite with hydrothermal synthesized manganese oxide
PANI-CoM	polyaniline composite with molten salt synthesized manganese oxide
PC	pseudocapacitance

SC	supercapacitor
SSC	symmetric supercapacitor
TEM	transmission electron microscope
TGA	thermogravimetric analysis
XRD	X-ray diffraction

DEVELOPMENT OF SUPERCAPACITORS WITH IN-SITU POLYMERIZED
POLYANILINE ON MnO_2 AND Co_3O_4 ANODES AND ACTIVATED CARBON
CATHODES

IZAN IZWAN BIN MISNON

Thesis submitted in fulfillment of the requirements for the
award of the degree of Doctor of Philosophy

Faculty of Industrial Sciences & Technology
UNIVERSITI MALAYSIA PAHANG

AUGUST 2016

ABSTRACT

Supercapacitors (SCs) store electrochemical energy at an electrode – electrolyte interface with high power density (P_D), fast recharge capability and long cycle life. The SCs are two types according to the charge storage mechanisms: electric double layer capacitors (EDLCs) and pseudocapacitors (PCs). Allotropes and polymorphs of carbon are choice to build EDLCs electrodes whereas PCs are built from nanostructured metal oxides, hydroxides, chalcogenides and conducting polymers. Broad objective of this doctoral research is to develop a SC device with PC as anode and EDLC as cathode – this type of devices are called asymmetric supercapacitors (ASCs). Popular PC electrodes such as MnO_2 and Co_3O_4 have poor electrical conductivity – making their composite with conducting polymers such as polyaniline (PANI) is proposed to be a superior PC electrode. In this research, MnO_2 and Co_3O_4 were synthesized by hydrothermal reaction and molten salt methods and their polymeric composite were developed by in situ polymerization. The materials were characterized by thermal analyses, X-ray and electron diffraction, FTIR spectroscopy, gas adsorption studies, scanning and transmission electron microscopy, and cyclic voltammetry. The electrochemical properties of the electrodes were evaluated systematically using cyclic voltammetry, galvanostatic charge–discharge cycling, and electrochemical impedance spectroscopy. The relationship between the pores in the electrodes and the size of the solvated ions in the electrolyte on the final capacitance in various aqueous electrolytes were investigated – the pores smaller than the size of the solvated ions do not contribute to the capacitance of the electrode. Aqueous KOH shown the best diffusion coefficient ($6.8 \times 10^{-10} \text{ cm}^2 \text{ s}^{-1}$) and capacitive properties in this study; therefore, it was chosen as the electrolyte of choice. The PANI provided faster ion channeling to the surface of metal oxides and showed improved charge storage capacity than their bare analogues. Highest specific capacitance (C_S) obtained in this study was in a PANI composite of Co_3O_4 synthesized by the molten salt method ($C_S \sim 985 \text{ F g}^{-1}$ at 2 mV s^{-1}), recording an increase of $\sim 253\%$ compared to its bare analogue. Three choice of EDLC electrodes were considered in this study, viz. (i) activated carbon from palm kernel shells (PKS) as it form a local abundant natural resource, (ii) commercial activated carbon (AC), and (iii) ordered mesoporous carbon (OMC). The PKS were pyrolyzed and activated using physical and chemical activation methods whereas the other two were obtained from commercial sources. Structural, thermal, morphological, surface, and electrochemical properties of the carbon electrodes were also systematically studied as done for the PC electrodes. The PKS activated carbon showed high areal capacitance ($\sim 45 \text{ } \mu\text{F cm}^{-2}$), which is one of the highest reported so far in literature, besides showing high cycle stability (95–97%). The ASCs were fabricated using the PC electrodes as anodes and carbons as cathodes. For MnO_2 series, PANI- MnO_2 (hydrothermal)//OMC recorded the highest energy density (E_D) $\sim 27 \text{ Wh kg}^{-1}$ at $P_D \sim 400 \text{ W kg}^{-1}$ whereas for Co_3O_4 series, PANI- Co_3O_4 (hydrothermal)//OMC gives E_D of $\sim 23 \text{ Wh kg}^{-1}$ at similar P_D . Despite its nominally smaller E_D , the Co_3O_4 based device showed superior cycling stability than the other.

ABSTRAK

Superkapasitor (SCs) menyimpan tenaga elektrokimia pada antara muka elektrod – elektrolit dan mempunyai ketumpatan kuasa (P_D) yang tinggi, pantas untuk pengecasan semula dan jangka hayat yang panjang. Menurut mekanisma simpanan cas, SC terdiri dari dua jenis: superkapasitor elektrik dua lapisan (EDLCs) dan pseudokapasitor (PCs). Alotrop dan polimorf karbon adalah pilihan untuk membangunkan elektrod EDLCs sementara PCs dibangunkan dari logam oksida berstruktur nano, hidroksida, chalcogenida dan polimer berkonduksi. Objektif luas kajian kedoktoran ini ialah membangunkan peranti SC dengan PC sebagai anod dan EDLC sebagai katod – peranti jenis ini dikenali sebagai superkapasitor asimetrik (ASCs). Elektrod PC yang popular seperti MnO_2 dan Co_3O_4 mempunyai konduksi elektrik yang lemah – di mana komposit dengan polimer berkonduksi seperti polianilin (PANI) dicadangkan untuk penghasilan elektrod PC yang lebih baik. Dalam kajian ini, MnO_2 dan Co_3O_4 disintesis dengan tindakbalas hidroterma dan kaedah garam lebur dan komposit polimer pula dibangunkan menggunakan kaedah pempolimeran in-situ. Bahan-bahan yang telah disintesis dicirikan menggunakan analisis terma, pembelauan electron dan sinar-X, spektroskopi FTIR, kajian penyerapan gas, mikroskopi imbasan dan transmisi elektron, dan voltametri berkitar. Sifat elektrokimia elektrod dinilai secara sistematik menggunakan voltammetry berkitar, kitaran cas–discas galvanostatik, dan spektroskopi impedans elektrokimia. Hubungkait antara liang elektrod dan saiz ion tersolvat dalam elektrolit terhadap kapasitan akhir dalam pelbagai elektrolit telah dikaji – liang bersaiz lebih kecil dari saiz ion tersolvat tidak menyumbang kepada kapasitan elektrod. KOH akuas menunjukkan koefisi difusi ($6.8 \times 10^{-10} \text{ cm}^2 \text{ s}^{-1}$) dan sifat kapasitan terbaik dalam kajian ini; oleh itu, ia dipilih sebagai elektrolit. PANI menghasilkan penyaliran ion yang cepat kepada permukaan logam oksida dan menunjukkan peningkatan kapasiti storan cas berbanding analog asal. Kapasitan spesifik (C_S) tertinggi yang direkodkan dalam kajian ini ialah komposit PANI dengan Co_3O_4 yang disintesis dengan kaedah logam lebur ($C_S \sim 985 \text{ F g}^{-1}$ at 2 mV s^{-1}), peningkatan $\sim 253\%$ berbanding analog asal. Tiga jenis elektrod EDLC diperincikan dalam kajian ini, iaitu (i) karbon taraktif dari tempurung kelapa sawit (PKS) memndangkan ia merupakan sumber semulajadi yang banyak didapati, (ii) karbon taraktif (AC) komersil dan (iii) karbon berliang meso tersusun (OMC). PKS dipirolisis dan diaktifkan menggunakan kaedah pengaktifan kimia dan fizik sementara dua lagi karbon diperolehi dari sumber komersil. Sifat struktur, terma, morfologi, permukaan dan elektrokimia elektrod karbon dikaji secara sistematik seperti yang dilakukan kepada elektrod PC. Karbon taraktif PKS menunjukkan kapasitan area yang tinggi ($45 \mu\text{F cm}^{-2}$), merupakan salah satu nilai tertinggi berbanding literatur, selain menunjukkan stabiliti kitaran yang tinggi (95 – 97%). Peranti ASCs yang difabrikasi menggunakan elektrod PC sebagai anod dan karbon sebagai katod. Untuk siri MnO_2 , PANI- MnO_2 (hidroterma)//OMC mencatatkan ketumpatan tenaga (E_D) tertinggi $\sim 27 \text{ Wh kg}^{-1}$ pada $P_D \sim 400 \text{ W kg}^{-1}$ sementara untuk siri Co_3O_4 , PANI- Co_3O_4 (hidroterma)//OMC memberikan $E_D \sim 23 \text{ Wh kg}^{-1}$ pada P_D yang sama. Walaupun mempunyai E_D yang kecil, peranti berasaskan Co_3O_4 menunjukkan stabiliti kitaran yang lebih baik berbanding elektrod lain.